One-phonon resonant Raman scattering of high frequency pseudocubic modes in zinc-blende-like tetragonal semiconductors

2004 J. Phys.: Condens. Matter 16 8353

(http://iopscience.iop.org/0953-8984/16/46/021)

INSTITUTE OF PHYSICS PUBLISHING JOURNAL OF PHYSICS: CONDENSED MATTER

J. Phys.: Condens. Matter **16** (2004) 8353–8366 PII: S0953-8984(04)79183-3

One-phonon resonant Raman scattering of high frequency pseudocubic modes in zinc-blende-like tetragonal semiconductors

J M Bergues[1] **and M L Sanjuán**

Instituto de Ciencia de Materiales de Aragón, Universidad de Zaragoza-CSIC, Facultad de Ciencias, 50009 Zaragoza, Spain

Received 14 April 2004, in final form 10 September 2004
Published 5 November 2004
Online at stacks.iop.org/JPhysCM/16/8353
doi:10.1088/0953-8984/16/46/021

Abstract

The one-phonon resonant Raman scattering of tetragonal zinc-blende-like semiconductors is presented and applied to II–III_2–VI_4 ordered-vacancy compounds, in particular to $ZnGa_2Se_4$. The well-known theory of one-phonon resonant Raman scattering in III–V or II–VI polar semiconductors has been extended to the tetragonal symmetry of these materials in the approximation that they can be considered as slightly distorted zinc-blende compounds. This approach is especially valid for the high frequency $B + E$ modes that arise from the zone centre optical mode of the zinc-blende structure and show, in an ordered-vacancy compound, a very small tetragonal splitting. The LO components of these modes, B_{LO} and E_{LO}, are considered. The contribution of the different excitonic transitions to the scattering process is studied. Deformation potential and Fröhlich interaction are considered as exciton–phonon interaction mechanisms. Emphasis is placed in the discussion on aspects related to symmetry lowering. Interference effects between excitonic resonances are also discussed.

1. Introduction

Resonant Raman scattering (RRS) has an advantage over other optical techniques in that it supplies simultaneously information about the electronic structure and the lattice dynamics of semiconductors. Raman selection rules allow the study of electron–phonon interaction and the separation of long-range (Fröhlich interaction (FI)) and short-range (deformation potential (DP)) electron–phonon interactions via symmetry considerations [1].

RRS by one LO phonon is a third-order process in which the energy of the photon is transferred to the lattice via intermediate electronic states. A theoretical model that gives a

[1] On leave from: Deparmento de Física, Universidad de Oriente, Santiago de Cuba 90500, Cuba.

good agreement with experimental measurements has been developed for the II–VI and III–V cubic semiconductors [2–4]. In a three-band model, using the hydrogenic approximation for the discrete–discrete, discrete–continuous, continuous–discrete and continuous–continuous exciton states, the Raman polarizability for the DP interaction was calculated [2]. In order to get the Raman polarizability for the FI, a two-band model with the same Wannier–Mott exciton as the intermediate electronic state was employed [3]. Effects of interference between FI and DP mechanisms were analysed too [3, 4]. The expressions derived from this theory are quite general. The choices of the envelope function and the Raman tensor for the zone centre optical phonons constitute the only approximation. In the framework of the virtual crystal approximation, where the cation potential is replaced by a weighted average of the cation potentials and disorder effects are not taken into account, these models have been used satisfactorily in several papers concerning zinc-blende alloys [5, 6].

As regards non-cubic systems, RRS has been applied in the vicinity of the fundamental absorption edge to investigate the electron–phonon interactions in the $AgGaSe_2$ chalcopyrite [7]. Enhancements in the cross sections of several one-phonon and multiphonon Raman bands at its lowest energy exciton were observed. In that work, the chalcopyrite band structure was considered as that of zinc-blende under a uniaxial strain along the [001] axis.

On the other hand, the II–III_2–VI_4 semiconductors or ordered-vacancy compounds (OVC), with space groups $I\bar{4}$ or $I\bar{4}2m$, have attracted attention because of their interesting optical and optoelectronic properties with potential applications. Among other techniques, Raman scattering has been widely used to study vibrational and structural properties [8]. In some of these works resonance enhancements have been reported. However, up to now, we have no knowledge of a theoretical treatment of the one-phonon resonant Raman scattering (OPRRS) in II–III_2–VI_4 semiconductors.

In this paper, we focus our attention on the OPRRS by optical phonons near the E_{g1}, E_{g2} and E_{g3} gaps in II–III_2–VI_4 semiconductors. The main assumption of our model is that in these compounds the following conditions are satisfied:

(a) the polar modes of highest frequency at the Brillouin zone centre arise from the zone centre mode of the cubic zinc-blende analogue [1],
(b) the polar modes with the highest energy are determined by the properties of the III–VI sublattices alone and are not influenced by the presence of the ordered array of vacancies [9],
(c) the electronic states at the top of the valence band arise mainly from anion p states and are not affected significantly by cation substitution or vacancies.

We take the tetragonal distortion to be along the [001] direction. Thus, the II–III_2–VI_4 compounds can be considered as a double zinc-blende unit cell deformed along the [001] direction and the theory of OPRRS in the II–VI and III–V semiconductors may be applied to the highest frequency polar mode with some modifications to account for the symmetry of the phonons and electronic states, the volume of the primitive cell and selection rules of the process. From the calculation of the Raman polarizability a strong enhancement of the one-phonon intensity is predicted when the photon energies are resonant with the free exciton. Differences with respect to the cubic case and interference effects are discussed.

The organization of this paper is as follows. In the next section, we will review briefly the relevant topics as regards the structural, optical and vibrational properties of II–III_2–VI_4 compounds. The energies and wavefunctions of the valence bands are determined as a function of a tetragonal crystal field parameter. In section 3, we will recall the theory of RRS in cubic tetrahedral semiconductors and will adapt it for II–III_2–VI_4 tetragonal compounds. Section 4 is devoted to results and discussion. The defect stannite $ZnGa_2Se_4$ is presented as an example.

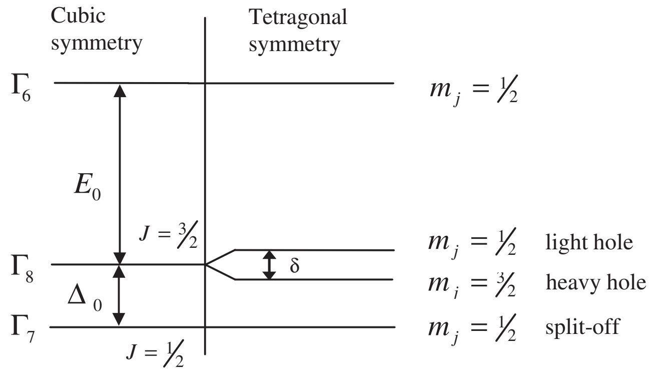

Figure 1. A schematic diagram of electronic states at the top (bottom) of the valence (conduction) bands of II–III_2–VI_4 compounds. This case corresponds to negative crystal field parameter. When the value of the crystal field parameter is positive, the ordering of light hole and heavy hole bands is interchanged.

Selection rules are worked out and the intensity dependence on excitation energy is discussed. Finally, the last section summarizes our conclusions.

2. Fundamentals topics

The tetragonal II–III_2–VI_4 compounds can be regarded as derived from the zinc-blende structure by successive cation substitution and the incorporation of an ordered array of vacancies in cationic sites. These changes yield a doubling of the unit cell along the c axis and a slight compression, so $c \leqslant 2a$.

In zinc-blende-type crystals, the lowest conduction band and the top valence band at the zone centre are identified with anti-bonding (s-symmetry) and bonding (p-symmetry) orbitals, respectively. The sixfold-degenerate zone centre valence bands (orbital symmetry Γ_{15}) are split by the spin–orbit interaction into a fourfold-degenerate Γ_8 state ($p_{3/2}$ multiplet; $J = 3/2$, $m_j = \pm 3/2, \pm 1/2$) and a doubly degenerate Γ_7 state ($p_{1/2}$ multiplet; $J = 1/2, m_j = \pm 1/2$) (see figure 1). When the crystal potential has tetragonal symmetry, the $J = 3/2$ multiplet is further split so that the higher lying states are either the heavy hole or the light hole ones, depending on the sign of the crystal field parameter. Thus, the fundamental absorption edge can be identified with light hole or heavy hole valence band states (see figure 1). In the materials under study the gap is a direct one. We therefore restrict our analysis to the Brillouin zone centre (Γ point).

We will consider the II–III_2–VI_4 semiconductors as zinc-blende-like materials distorted along the [001] axis and built of two sublattices: a cationic (cations plus ordered vacancies) and an anionic one in which the properties of the polar modes of highest frequency are determined only by III–VI sublattices. This assertion derives from many experimental results, from which it is found that substitution of the divalent cation does not affect the energy of the high frequency mode while it is modified by a change in either the trivalent cation or in the anion. The different structures that can be formed according to the cation distribution have been described in [10]. Since the tetragonal distortion is small, we assume that the states at the bottom (top) of the conduction (valence) bands can be identified with states of s and p symmetry, respectively, as in the zinc-blende lattice. Then we will assume parabolic bands and, in the framework of the envelope-function approximation, the hydrogenic model.

We now describe how the lower symmetry affects the top valence bands. For these states the Hamiltonian can be written as

$$\hat{H} = \hat{H}_{so} + \hat{H}_{cf},$$

$\hat{H}_{so}$ being the spin–orbit Hamiltonian and $\hat{H}_{cf}$ the crystal field potential that accounts for the tetragonal distortion at $\vec{\mathbf{k}} = 0$. Taking the latter to be along the [001] direction, its expression is given by

$$\hat{H}_{cf} = -\tfrac{3}{2}\delta\left[\hat{L}_z^2 - \tfrac{1}{3}\hat{L}^2\right], \tag{1}$$

where $\hat{L}$ is the angular momentum operator and $\hat{L}_z$ its z component. With this definition of $\hat{H}_{cf}$, the crystal field parameter δ gives the linear splitting of the $J = 3/2$ multiplet.

From the three factors that characterize the tetragonal symmetry of OVC (tetragonal distortion, cationic asymmetry and anionic displacement) [10], it has been found that the tetragonal crystal field potential, in the quasicubic model, is dominated by the tetragonal distortion [11]. Then, δ can be written as

$$\delta = \tfrac{3}{2}b_{DP}(2 - c/a), \tag{2}$$

where b_{DP} is a typical DP parameter of the corresponding binary compound and $2 - c/a$ is a measure of the tetragonal distortion.

For convenience, we will use the same notation as Pollak and Cardona in [12]. For a zinc-blende crystal the wavefunctions of the valence band, in the (J, m_j) representation along the [001] direction, and the conduction band can be written as [2]

$$\begin{aligned}
\left|\frac{3}{2},+\frac{3}{2}\right\rangle_{001} &= \frac{1}{\sqrt{2}}\left|(X+\mathrm{i}Y)\uparrow\right\rangle, & \left|\frac{3}{2},-\frac{3}{2}\right\rangle_{001} &= \frac{1}{\sqrt{2}}\left|(X-\mathrm{i}Y)\downarrow\right\rangle,\\
\left|\frac{3}{2},+\frac{1}{2}\right\rangle_{001} &= \frac{1}{\sqrt{6}}\left|(X+\mathrm{i}Y)\downarrow -2Z\uparrow\right\rangle, & \left|\frac{3}{2},-\frac{1}{2}\right\rangle_{001} &= \frac{1}{\sqrt{6}}\left|(X-\mathrm{i}Y)\uparrow +2Z\downarrow\right\rangle,\\
\left|\frac{1}{2},+\frac{1}{2}\right\rangle_{001} &= \frac{1}{\sqrt{3}}\left|(X+\mathrm{i}Y)\downarrow +Z\uparrow\right\rangle, & \left|\frac{1}{2},-\frac{1}{2}\right\rangle_{001} &= \frac{1}{\sqrt{3}}\left|(X-\mathrm{i}Y)\uparrow -Z\downarrow\right\rangle,\\
\left|\frac{1}{2},+\frac{1}{2}\right\rangle &= \left|S\uparrow\right\rangle, & \left|\frac{1}{2},-\frac{1}{2}\right\rangle &= \left|S\downarrow\right\rangle,
\end{aligned} \tag{3}$$

$\uparrow$ ($\downarrow$) indicating spin up (down). X, Y and Z (S) are the valence band (conduction band) wavefunctions which transform as atomic p (s) functions under the operations of the group of the tetrahedron.

Since the tetragonal crystal field does not remove the Kramers degeneracy of each state, from equations (1)–(3) the Hamiltonian matrix for the valence bands has the following form:

$$\begin{array}{c}
\begin{array}{ccc} \left|\tfrac{3}{2},+\tfrac{3}{2}\right\rangle_{001} & \left|\tfrac{3}{2},+\tfrac{1}{2}\right\rangle_{001} & \left|\tfrac{1}{2},+\tfrac{1}{2}\right\rangle_{001} \end{array}\\
\begin{pmatrix}
\tfrac{1}{3}\Delta_0 - \tfrac{1}{2}\delta & 0 & 0\\
0 & \tfrac{1}{3}\Delta_0 + \tfrac{1}{2}\delta & -\tfrac{\sqrt{2}}{2}\delta\\
0 & -\tfrac{\sqrt{2}}{2}\delta & -\tfrac{2}{3}\Delta_0
\end{pmatrix}
\end{array}, \tag{4}$$

Δ_0 being the spin–orbit splitting. From the above Hamiltonian, the energies of the valence bands can be calculated as follows:

$$\begin{aligned}
E_1 &= -\tfrac{1}{6}\Delta_0 + \tfrac{1}{4}\delta + \tfrac{1}{2}\sqrt{\Delta_0^2 + \Delta_0\delta + \tfrac{9}{4}\delta^2},\\
E_2 &= \tfrac{1}{3}\Delta_0 - \tfrac{1}{2}\delta,\\
E_3 &= -\tfrac{1}{6}\Delta_0 + \tfrac{1}{4}\delta - \tfrac{1}{2}\sqrt{\Delta_0^2 + \Delta_0\delta + \tfrac{9}{4}\delta^2}.
\end{aligned} \tag{5}$$

When $\delta \ll \Delta_0$, equation (5) can be expanded in powers of δ/Δ_0:

$$\begin{aligned} E_1 &= \frac{1}{3}\Delta_0 + \frac{1}{2}\delta + \frac{1}{2}\frac{\delta^2}{\Delta_0} + \cdots, && \text{(lh)} \\ E_2 &= \frac{1}{3}\Delta_0 - \frac{1}{2}\delta, && \text{(hh)} \\ E_3 &= -\frac{2}{3}\Delta_0 - \frac{1}{2}\frac{\delta^2}{\Delta_0} + \cdots, && \text{(so)} \end{aligned} \tag{6}$$

and the wavefunctions of the valence band states at $\vec{k} = 0$ are obtained in first order as

$$\begin{aligned} v_1^{\pm} &= \left|\frac{3}{2}, \pm\frac{1}{2}\right\rangle_{001} - \frac{\alpha_0}{\sqrt{2}}\left|\frac{1}{2}, \pm\frac{1}{2}\right\rangle_{001} && \text{(lh)} \\ v_2^{\pm} &= \left|\frac{3}{2}, \pm\frac{3}{2}\right\rangle_{001} && \text{(hh)} \\ v_3^{\pm} &= \left|\frac{1}{2}, \pm\frac{1}{2}\right\rangle_{001} + \frac{\alpha_0}{\sqrt{2}}\left|\frac{3}{2}, \pm\frac{1}{2}\right\rangle_{001}, && \text{(so)} \end{aligned}$$

where $\alpha_0 = \delta/\Delta_0$. If the condition $\delta \ll \Delta_0$ is not satisfied, the energies and wavefunctions can be determined from the diagonalization of the Hamiltonian matrix (4).

3. The theory of one-phonon RRS in II–III$_2$–VI$_4$ semiconductors

We will give theoretical expressions for a OPRRS process in which the exciton–phonon interaction occurs via DP and FI. For clarity, we will use the same notation as in [2] and [3]. Under the assumption of small distortion and a quasicubic mode, the expressions given in these works for the Raman polarizability in the cubic case are also valid for tetragonal systems, provided that tetragonality is introduced as appropriate:

(i) hh and lh valence bands are split and thus we must consider three gaps instead of two;
(ii) the threefold-degenerate zone centre mode of the zinc-blende structure is split into a singlet and a doublet ($B_2 + E$, in the $I\bar{4}2m$ systems), that must be handled separately.

3.1. Raman polarizability

To calculate the OPRRS, we consider a model with parabolic bands and correlated electron–hole pairs as excited states. The Raman scattering intensities are displayed as squared Raman polarizabilities. These independent components of the Raman tensor are related to the probability amplitude $W_{\rm FI}$ for the transition between an initial state $|{\rm I}\rangle$ and a final state $|{\rm F}\rangle$ through [13]

$$\vec{e}_{\rm s} \cdot \overleftrightarrow{R} \cdot \vec{e}_{\rm L} = \frac{\eta_{\rm L}\eta_{\rm s}}{2\pi}\frac{V_{\rm c}}{\bar{u}_0}\frac{1}{\hbar\omega_{\rm L}} W_{\rm FI}(\omega_{\rm s}, \vec{e}_{\rm s}; \omega_{\rm L}, \vec{e}_{\rm L}),$$

where $\eta_{\rm s}$ ($\eta_{\rm L}$) is the refraction index for scattered (incident) light with frequency $\omega_{\rm s}$ ($\omega_{\rm L}$) and vector polarization $\vec{e}_{\rm s}$ ($\vec{e}_{\rm L}$), $V_{\rm c}$ is the volume of the primitive cell and $\bar{u}_0$ is the relative displacement of ions vibrating in a zinc-blende-like optical mode with frequency ω_0.

Considering only the term that dominates near resonance, for a one-phonon process the probability amplitude can be expressed as

$$W_{\mathrm{FI}} = \sum_{p,q}\left[\frac{\langle F|\hat{H}_{\mathrm{ER}}|q\rangle\langle q|\hat{H}_{\mathrm{EL}}|p\rangle\langle p|\hat{H}_{\mathrm{ER}}|\mathrm{I}\rangle}{(\hbar\omega_{\mathrm{L}} - E_p + \mathrm{i}\Gamma_p)(\hbar\omega_{\mathrm{s}} - E_q + \mathrm{i}\Gamma_q)}\right].$$

The indices p and q refer to excitonic intermediate states with energies and lifetime broadening parameters E_p, Γ_p and E_q, Γ_q, respectively. $\hat{H}_{\mathrm{EL}}$ is the exciton–phonon interaction Hamiltonian containing $\hat{H}_{\mathrm{DP}}$ and $\hat{H}_{\mathrm{F}}$, the Hamiltonians for DP and FI, respectively, that we discuss below. $\hat{H}_{\mathrm{ER}}$ is the exciton–radiation interaction Hamiltonian that can be written as [13]

$$\hat{H}_{\mathrm{ER}} = \sum_{p,\vec{K},\vec{e},\vec{\kappa}}\left\{T^{p}_{cv}(\vec{K})D^{\dagger}_{p\vec{K}}(a_{\vec{\kappa},\vec{e}} + a^{\dagger}_{-\vec{\kappa},\vec{e}}) + [T^{p}_{cv}(\vec{K})]^{*}D_{p\vec{K}}(a_{\vec{\kappa},\vec{e}} + a^{\dagger}_{-\vec{\kappa},\vec{e}})\right\},$$

where $\vec{\kappa}$ is the wavevector of light; $\vec{K}$ is the centre-of-mass momentum of the exciton; $D^{\dagger}_{p\vec{K}}$ ($D_{p\vec{K}}$) and $a^{\dagger}_{-\vec{\kappa},\vec{e}}$ ($a_{\vec{\kappa},\vec{e}}$) are creation (annihilation) operators for excitons and photons, respectively. The exciton–photon coupling constants are given by [14]

$$T^{p}_{cv}(\vec{K}) = -\frac{e}{m_0}\left(\frac{2\pi\hbar}{\omega_\lambda\eta^2_\lambda}\right)^{1/2}\vec{e}\cdot\langle c|\vec{p}|v\rangle\psi_p(0)\delta_{\vec{K},\vec{\kappa}},$$

where λ is equal to L or s; e and m_0 are the free-electron charge and mass; $\psi_p(\vec{r})$ is the internal exciton wavefunction and $\langle c|\vec{p}|v\rangle$ is the matrix element of the momentum operator $\vec{p}$ connecting conduction and valence band states $|c\rangle$, $|v\rangle$, respectively.

3.2. Dipole-allowed DP interaction

To calculate the Raman polarizabilities, we consider first the dipole-allowed DP interaction. We use a three-band model involving two valence bands (v_p and v_q) and one conduction band (c). We reproduce from [2] the final expression for the Raman polarizability for DP interaction, using the hydrogenic approximation for the discrete and continuous exciton states and assuming the same Bohr radius for all excitons [2]:

$$\begin{aligned}\hat{e}_{\mathrm{s}}\cdot\overleftrightarrow{R}^{\mathrm{DP}}\cdot\hat{e}_{\mathrm{L}} = \sum_{p,q}K^{\mathrm{DP}}_{q,p}\Bigg\{&\sum_{n=1}^{\infty}\frac{1}{2n^3}\frac{1}{\left(\eta_p + 1/n^2 + \mathrm{i}\gamma_p\right)\left(\eta_q - \eta_0 + 1/n^2 + \mathrm{i}\gamma_q\right)}\\ &+ \frac{1}{4(\eta_0 + \eta_p - \eta_q + \mathrm{i}[\gamma_p(k) - \gamma_q(k)])}\Bigg\{\ln\left(\frac{\eta_q - \eta_0 + \mathrm{i}\gamma_q(k)}{\eta_p + \mathrm{i}\gamma_p(k)}\right)\\ &+ \pi\mathrm{i}\left[\coth\left[\frac{\pi}{\sqrt{\eta_p + \mathrm{i}\gamma_p(k)}}\right] - \coth\left[\frac{\pi}{\sqrt{\eta_q - \eta_0 + \mathrm{i}\gamma_q(k)}}\right]\right]\Bigg\}\Bigg\}\end{aligned} \tag{7}$$

with

$$\eta_p = \frac{\hbar\omega_{\mathrm{L}} - E_{\mathrm{g}p}}{R_p}, \qquad \eta_0 = \frac{\hbar\omega_0}{R_p}, \qquad \gamma_p = \frac{\Gamma_p}{R_p},$$

where R_p is the exciton Rydberg and $E_{\mathrm{g}p}$ the gap related to exciton p. The sum in p, q runs over heavy hole (hh), light hole (lh) and split-off (so) excitons. The factor $K^{\mathrm{DP}}_{q,p}$ is equal to

$$K^{\mathrm{DP}}_{q,p} = \frac{V_{\mathrm{c}}}{2\pi m_0 a_0}\frac{R^2_{\mathrm{H}}\sqrt{3}}{R^2}\frac{a^3_{\mathrm{H}}}{a^3_{\mathrm{B}}}\frac{\langle c|\vec{e}_{\mathrm{s}}\cdot\vec{p}|v_q\rangle\langle v_q|D_{\mathrm{h}}|v_p\rangle\langle v_p|\vec{e}_{\mathrm{L}}\cdot\vec{p}|c\rangle}{\hbar\omega_{\mathrm{L}}\sqrt{\hbar\omega_{\mathrm{L}}\hbar\omega_{\mathrm{s}}}}, \tag{8}$$

where $|v_p\rangle$, $|v_q\rangle$ and $|c\rangle$ are the Bloch functions at $\vec{k} = 0$ of the valence and conduction bands, respectively, corresponding to excitons p and q. a_{H} and R_{H} are the Bohr radius and Rydberg energy of the hydrogen atom, respectively, a_{B} is the exciton Bohr radius and a_0 is an average, cubic-like lattice parameter. D_{h} are the tensorial components of the DP interaction. The assumption of the same Bohr radius for all excitons has been justified in [2] for cubic

Table 1. Matrix elements EM $= \langle c|\vec{e}_s \cdot \vec{p}|v_q\rangle\langle v_q|D_h|v_p\rangle\langle v_p|\vec{e}_L \cdot \vec{p}|c\rangle$ for several scattering configurations on the (001) and (100) faces of tetragonal systems when the transitions $v_p \to v_q$ occur via DP interaction. $l = 1, 2$ and 3 correspond to lh, hh and so excitons, respectively. $P = \langle S|p_x|X\rangle = \langle S|p_y|Y\rangle$ and $P_z = \langle S|p_z|Z\rangle$.

l	$v_p \to v_q$	$B_{2(z)}$, $\bar{z}(x, y)z$ EM	$E_{(x)}$, $\bar{x}(y, z)x$ EM
1	$v_1 \to v_2$	$\frac{d_0}{6}P^2(1-\alpha_0)^2$	0
1	$v_1 \to v_3$	0	$\frac{d_0}{6}P_z P(1-\alpha_0)^2\left(1-\frac{\alpha_0^2}{2}\right)$
2	$v_2 \to v_1$	$\frac{d_0}{6}P^2(1-\alpha_0)^2$	$\frac{d_0}{3}P_z P\left(1+\frac{\alpha_0}{2}\right)^2$
2	$v_2 \to v_3$	$\frac{d_0}{3}P^2\left(1+\frac{\alpha_0}{2}\right)^2$	$\frac{d_0}{6}P_z P(1-\alpha_0)^2$
3	$v_3 \to v_1$	0	$\frac{d_0}{3}P_z P\left(1+\frac{\alpha_0}{2}\right)^2\left(1+\frac{\alpha_0^2}{2}\right)$
3	$v_3 \to v_2$	$\frac{d_0}{3}P^2\left(1+\frac{\alpha_0}{2}\right)^2$	0

systems. In this approximation the continuous–discrete and discrete–continuous contributions are equal to zero [2]. The first term on the right-hand side in equation (7) corresponds to the discrete–discrete excitonic transition and the last one to continuous–continuous contributions.

The selection rules for OPRRS processes are determined by the matrix elements

$$\langle c|\vec{e}_s \cdot \vec{p}|v_q\rangle\langle v_q|D_h|v_p\rangle\langle v_p|\vec{e}_l \cdot \vec{p}|c\rangle. \tag{9}$$

The DP operators D_h corresponding to each mode, when acting on $|X\rangle$, $|Y\rangle$, $|Z\rangle$ electronic states, have the same form as the Raman tensors for the zone centre optical phonons, that for B_2 and E modes in $I\bar{4}2m$ symmetry can be written as [1]

$$B_{2(z)} = \begin{pmatrix} & d & \\ d & & \\ & & \end{pmatrix}, \qquad E_{(y)} = \begin{pmatrix} & & e \\ & & \\ e & & \end{pmatrix}, \qquad E_{(x)} = \begin{pmatrix} & & \\ & & e \\ & e & \end{pmatrix}.$$

The E modes are twofold degenerate. The index in brackets stands for the phonon polarization direction. In table 1 we give the values of the matrix elements in equation (9) for a tetragonal system such as $ZnGa_2Se_4$ when the exciton–phonon interaction occurs via DP.

3.3. Dipole-forbidden Fröhlich interaction

In the framework of the envelope-function approximation and the hydrogenic model, the Raman polarizability for a FI two-band process is given by the following expression [3]:

$$\begin{aligned} a_F = \sum_p K_p^F \Bigg[& \sum_{n,m} \frac{D_{n,m}}{(\eta_p + 1/n^2 + i\gamma_n)(\eta_p - \eta_0 + 1/m^2 + i\gamma_m)} \\ & + \sum_n \int_0^\infty \frac{D_{n,k}}{1 - e^{-2\pi/k}} \frac{1}{n^3} \Bigg[\frac{1}{(\eta_p - k^2 + i\gamma(k))(\eta_p - \eta_0 + 1/n^2 + i\gamma_n)} \\ & + \frac{1}{(\eta_p + 1/n^2 + i\gamma_n)(\eta_p - \eta_0 - k^2 + i\gamma(k))} \Bigg] dk \end{aligned}$$

$$+\frac{\mathrm{i}}{8(Q_\mathrm{e}^2-Q_\mathrm{h}^2)}\left[\frac{1}{Q_\mathrm{e}}\ln\left(\frac{\sqrt{\eta_p+\mathrm{i}\gamma(k)}+\sqrt{\eta_p-\eta_0+\mathrm{i}\gamma(k)}-Q_\mathrm{e}}{\sqrt{\eta_p+\mathrm{i}\gamma(k)}+\sqrt{\eta_p-\eta_0+\mathrm{i}\gamma(k)}+Q_\mathrm{e}}\right)\right.$$
$$\left.\left.-\frac{1}{Q_\mathrm{h}}\ln\left(\frac{\sqrt{\eta_p+\mathrm{i}\gamma(k)}+\sqrt{\eta_p-\eta_0+\mathrm{i}\gamma(k)}-Q_\mathrm{e}}{\sqrt{\eta_p+\mathrm{i}\gamma(k)}+\sqrt{\eta_p-\eta_0+\mathrm{i}\gamma(k)}+Q_\mathrm{e}}\right)\right]\right], \qquad (10)$$

where the sum in p runs over hh, lh and so excitons. The coefficients are given by

$$D_{n,m}=\frac{1}{nm}\frac{I_{n,m}(-Q_\mathrm{h})-I_{n,m}(Q_\mathrm{e})}{Q_\mathrm{e}^2-Q_\mathrm{h}^2},$$

$$D_{n,k}=\frac{I_{n,k}(-Q_\mathrm{h})-I_{n,k}(Q_\mathrm{e})}{Q_\mathrm{e}^2-Q_\mathrm{h}^2},$$

$$K_p^\mathrm{F}=\frac{2}{\pi}\sqrt{\frac{a^2cM^*\hbar\omega_0}{m_0R_\mathrm{H}}}\frac{Qa_\mathrm{H}}{\hbar\omega_l\sqrt{\hbar\omega_l\hbar\omega_\mathrm{s}}}\frac{\langle c|\vec{e}_\mathrm{L}\cdot\vec{p}|v_p\rangle\langle v_p|\vec{e}_\mathrm{s}\cdot\vec{p}|c\rangle}{m_0}\frac{a_\mathrm{H}}{a_\mathrm{B}}\left(\frac{R_\mathrm{H}}{R}\right)^2C_\mathrm{F}^*\frac{m_\mathrm{e}-m_\mathrm{h}}{m_\mathrm{e}+m_\mathrm{h}},$$

with

$$I_{n,m}=\frac{-4}{Q_\alpha[(m-n)^2+n^2m^2Q_\alpha^2]}F\left(1-m,1-n,2,\frac{-4mn}{(m-n)^2+n^2m^2Q_\alpha^2}\right)$$
$$\times\ \mathrm{Im}\left[\left(\frac{m-n-\mathrm{i}nmQ_\alpha}{m+n-\mathrm{i}mnQ_\alpha}\right)^m\left(\frac{n-m-\mathrm{i}Q_\alpha mn}{n+m-\mathrm{i}Q_\alpha mn}\right)^n\right]$$

$$I_{n,k}=\frac{4k}{Q_\alpha}(-1)^{n-1}n^2\,\mathrm{Im}\left[\frac{F(1-n,1+\mathrm{i}/k,2,z)}{[1-\mathrm{i}n(k-Q_\alpha)][1-\mathrm{i}n(k+Q_\alpha)]}\right.$$
$$\left.\times\left(\frac{[1-\mathrm{i}n(k-Q_\alpha)]^{2n}}{[1+n^2(k-Q_\alpha)^2]^n}\left(\frac{1+\mathrm{i}n(k-Q_\alpha)}{1-\mathrm{i}n(k+Q_\alpha)}\right)^{\mathrm{i}/k}\right)\right],$$

where F is the hypergeometric function, $\vec{Q}_\alpha=(m_\alpha/(m_\mathrm{e}+m_\mathrm{h}))\vec{Q}a_\mathrm{B}$ and $\vec{Q}$ is the phonon wavevector. The Fröhlich constant C_F is given by $C_\mathrm{F}=-\mathrm{i}(\varepsilon_\infty^{-1}-\varepsilon_0^{-1})^{1/2}(2\pi\hbar\omega_0e^2)^{1/2}$, where ε_∞ and ε_0 are the optical and static dielectric constants, respectively, that we assume to be isotropic. m_e and m_h are the electron and hole effective masses, respectively.

The first term inside the second set of large parentheses in equation (10) represents the contribution of the discrete exciton states, the second and third terms correspond to continuous–discrete and discrete–continuous transitions and the last one is due to the continuous states. The most important contributions to the Raman tensor come from discrete–continuous plus continuous–discrete exciton terms [3].

The selection rules for OPRRS process are obtained from the matrix elements

$$\langle c|\vec{e}_\mathrm{L}\cdot\vec{p}|v_p\rangle\langle v_p|\vec{e}_\mathrm{s}\cdot\vec{p}|c\rangle \qquad (11)$$

in K_p^F. These yield Raman tensors for forbidden FI in $I\bar{4}2m$ symmetry of the form [1]

$$B_{2(z)}^F=\begin{pmatrix}d_\mathrm{F}&&\\&d_\mathrm{F}&\\&&d'_\mathrm{F}\end{pmatrix},\qquad E_{(y)}^F=\begin{pmatrix}e_\mathrm{F}&&\\&e_\mathrm{F}&\\&&e'_\mathrm{F}\end{pmatrix},\qquad E_{(x)}^F=\begin{pmatrix}e_\mathrm{F}&&\\&e_\mathrm{F}&\\&&e'_\mathrm{F}\end{pmatrix}.$$

Matrix elements for FI are given in table 2.

4. Results and discussion

With the preceding equations we have calculated the Raman polarizability for the highest frequency B_LO and E_LO pseudocubic modes of $ZnGa_2Se_4$ ($\approx$286 cm^{-1}) in several

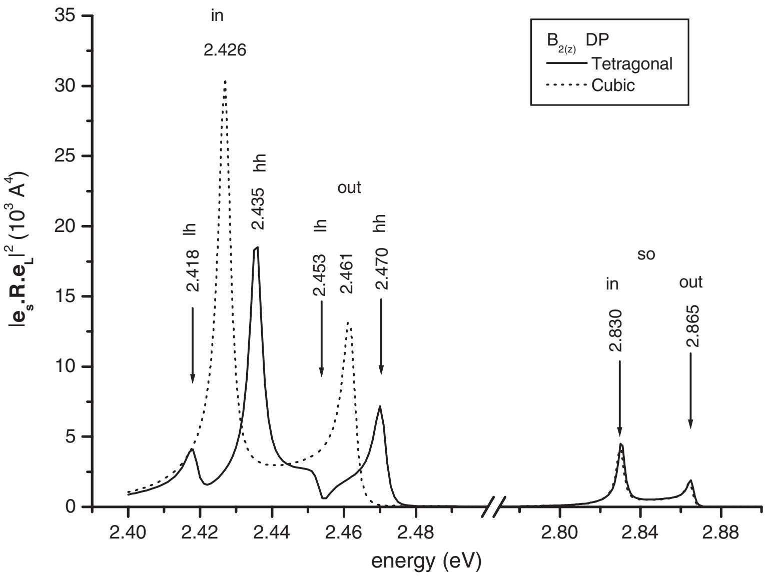

Figure 2. Raman polarizability for the $B_{2(z)}$ mode of $ZnGa_2Se_4$ in the $z(xy)\bar{z}$ configuration when the exciton–phonon interaction occurs via DP. The solid (dotted) curve corresponds to a tetragonal (cubic) crystal field. The incoming (in) and outgoing (out) resonances for lh, hh and so excitons are indicated for $n = 1$. The broadening parameter $\Gamma_p(1)$ is equal to 2 meV for all excitons.

Table 2. Matrix elements $EM = \langle c|\vec{e_s}\cdot\vec{p}|v_p\rangle\langle v_p|\vec{e_L}\cdot\vec{p}|c\rangle$ for several scattering configurations on the (001) and (100) faces when the transitions $v_p \to v_q$ occur via Fröhlich interaction. $l = 1, 2$ and 3 correspond to lh, hh and so excitons, respectively. $P = \langle S|p_x|X\rangle = \langle S|p_y|Y\rangle$ and $P_z = \langle S|p_z|Z\rangle$.

l	$v_p \to v_p$	$B_{2(z)}, \bar{z}(x,x)z$ EM	$E_{(x)}, \bar{x}(z,z)x$ EM	$E_{(x)}, \bar{x}(y,y)x$ EM
1	$v_1 \to v_1$	$\frac{1}{6}P^2(1-\alpha_0)^2$	$\frac{2}{3}P_z^2\left(1+\frac{\alpha_0}{2}\right)^2$	$\frac{1}{6}P^2(1-\alpha_0)^2$
2	$v_2 \to v_2$	$\frac{1}{2}P^2$	0	$\frac{1}{2}P^2$
3	$v_3 \to v_3$	$\frac{1}{3}P^2\left(1+\frac{\alpha_0}{2}\right)^2$	$\frac{1}{3}P_z^2(1-\alpha_0)^2$	$\frac{1}{3}P^2\left(1+\frac{\alpha_0}{2}\right)^2$

backscattering configurations on the (001) and (100) planes. In the selected configurations the B_{LO} or E_{LO} character is exact, in the sense that no symmetry or character mixing occurs, i.e., the formalism of oblique phonons for uniaxial media is not necessary.

The selection rules of the processes can be determined from expressions (9) and (11) for the DP and FI, respectively. The results are presented in tables 1 and 2, in which $P = 2\pi\hbar/a$ and $P_z = 2\pi\hbar/c_z$ with $c_z = c/2$. From table 1, we can see the different behaviour of mode E_{LO} in configuration $\bar{x}(y,z)x$ relative to that of B_{LO} in configuration $\bar{z}(x,y)z$. In contrast, from table 2, we can note that mode B_{LO} in the $\bar{z}(x,x)z$ configuration has the same behaviour as E_{LO} in the $\bar{x}(y,y)x$ configuration but different to that of E_{LO} in the $\bar{x}(z,z)x$ configuration.

The Raman polarizabilities for LO phonons in $ZnGa_2Se_4$ as a function of incident energy are shown in figures 2–5. The incoming and outgoing resonances are indicated by ‘in’ and ‘out’, respectively, the difference between them being equal to the phonon energy, 0.035 eV.

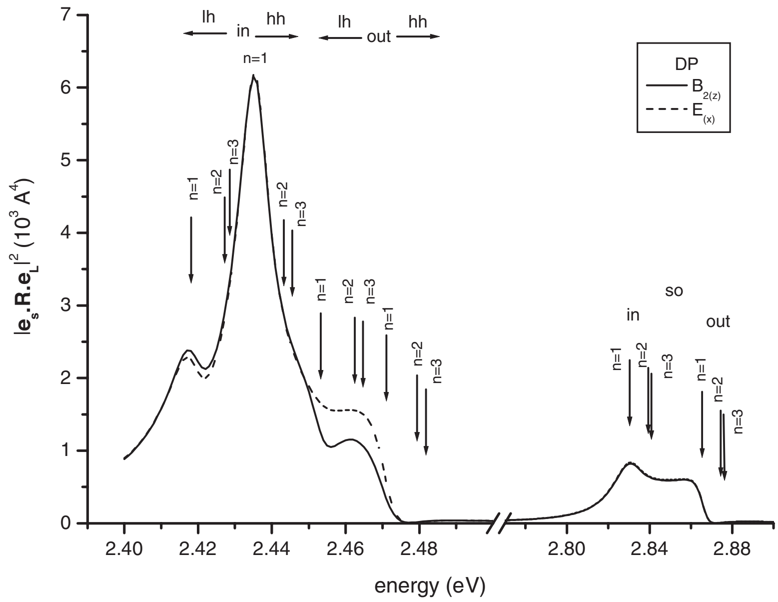

Figure 3. Raman polarizability for $B_{2(z)}$ (solid curve) and $E_{(x)}$ (dashed curve) modes of $ZnGa_2Se_4$ in $z(xy)\bar{z}$ and $x(yz)\bar{x}$ configurations, respectively, when the exciton–phonon interaction occurs via DP. The broadening parameters are $\Gamma_{lh}(1) = \Gamma_{hh}(1) = 5$ meV, $\Gamma_{so}(1) = 10$ meV. The incoming (in) and outgoing (out) resonances are indicated for $n = 1$, 2 and 3.

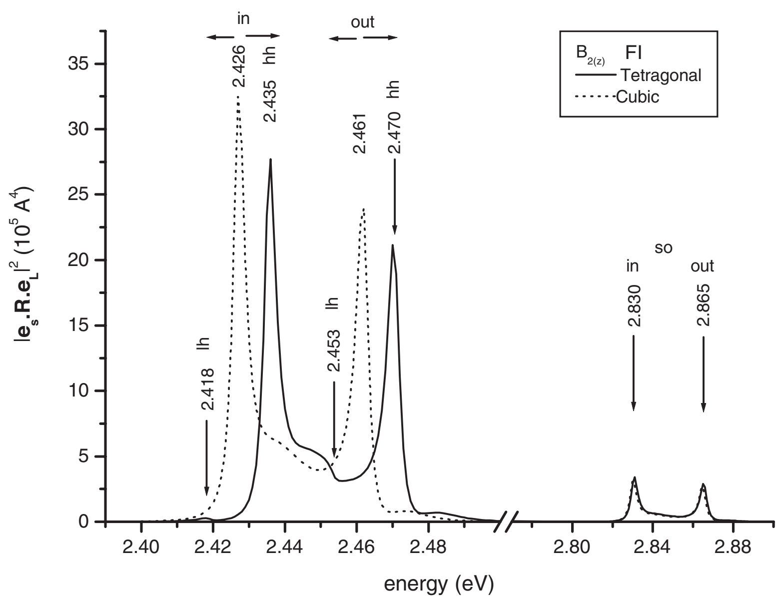

Figure 4. Raman polarizability for the $B_{2(z)}$ mode of $ZnGa_2Se_4$ in the $z(xx)\bar{z}$ configuration when the exciton–phonon interaction is of Fröhlich type. The solid (dotted) curve corresponds to a tetragonal (cubic) crystal field. The incoming (in) and outgoing (out) resonances for lh, hh and so exciton transitions are indicated for $n = 1$. The broadening parameter $\Gamma_p(1)$ is equal to 2 meV for all excitons.

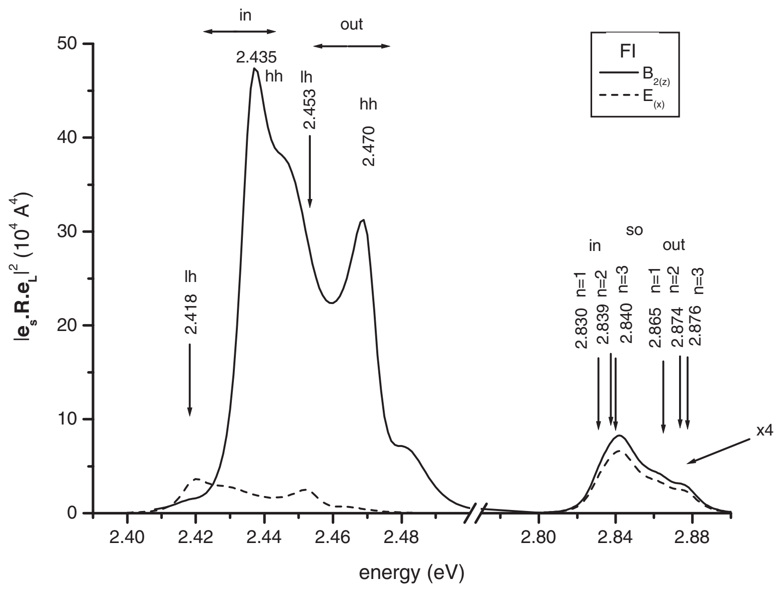

Figure 5. Raman polarizability for $B_{2(z)}$ (solid curve) and $E_{(x)}$ (dashed curve) modes of $ZnGa_2Se_4$ in $z(xx)\bar{z}$ and $x(zz)\bar{x}$ configurations, respectively, when the exciton–phonon interaction occurs via FI. The broadening parameters are $\Gamma_{\mathrm{lh}}(1) = \Gamma_{\mathrm{hh}}(1) = 5$ meV, $\Gamma_{\mathrm{so}}(1) = 10$ meV. The incoming (in) and outgoing (out) resonances are indicated for $n = 1, 2$ and 3.

In all cases, the Raman intensity decreases when n increases, as results from equations (7) (for DP) and (10) (for FI). The contributions of heavy hole, light hole and split-off excitons are added before squaring, allowing for interference effects between them. These contributions are indicated by hh, lh and so, respectively. In order to evaluate the lifetime we have used the following empirical relation:

$$\Gamma_p(n) = \Gamma_p(k) - \frac{[\Gamma_p(k) - \Gamma_p(1)]}{n^2}. \qquad (12)$$

Since we lack experimental data, the values of the broadening parameters are arbitrarily assumed. We have taken $\Gamma_p(k) = 10$ meV for all continuum excitons; $\Gamma_{\mathrm{hh}}(1)$, $\Gamma_{\mathrm{lh}}(1)$ and $\Gamma_{\mathrm{so}}(1)$ are given either the same or different values, varying with p. The Rydberg energies R_{hh}, R_{lh} and R_{so} have been taken to be equal. We will also assume that the valence band masses are isotropic. In such cases heavy and light hole effective masses can be obtained by averaging over all possible directions of k and the electron effective one is approximately equal to $P^2/(2m_0)\mathrm{E}_{\mathrm{g1}}$ [15]. The physical parameters used in the calculations are summarized in table 3.

Figure 2 depicts the dependence on the excitation energy of the dipole-allowed DP Raman intensity for mode B_{LO} in the $\bar{z}(x, y)z$ configuration. In order to stress the contribution of each term, the lifetime parameters $\Gamma_p(1)$ ($p = $ hh, lh, so) have been taken equal and small (2 meV). The calculation for the tetragonal case is compared to that for cubic symmetry, obtained in the limit $\delta \to 0$. In the cubic limit (dotted line) the most intense peaks correspond to incoming and outgoing resonances of $n = 1$ excitons of lh + hh and so states. With our parameters, the incoming resonance is more intense than the outgoing one. The tetragonal crystal field produces a splitting between the lh and hh resonances of magnitude equal to the linear crystal field splitting, 0.017 eV. As expected, no difference is found in the region of the split-off exciton that is, in first order, independent of the tetragonal crystal field. The

Table 3. Numerical values of the physical parameters for $ZnGa_2Se_4$ used in this work.

Parameter	Value	Parameter	Value
ε_0 [5]	9	m_e [a]	0.12 m_0
ε_∞ [5]	5.5	m_{hh} [a]	0.77 m_0
R_{lh}	11.5 meV	m_{lh} [a]	0.16 m_0
E_{g1} [19]	2.43 eV	m_{so} [5]	0.28 m_0
Δ_0 [5]	0.403 eV	$\hbar\omega_{LO}$ [8]	35 meV
b_{DP} [15]	−1.2 eV		

[a] Estimated from [15].

energies 2.418 and 2.453 eV correspond to incoming and outgoing contributions of $n = 1$ lh excitons; 2.435 and 2.470 eV are those corresponding to the hh. The positions of $n = 2$ and 3 excitons are not indicated for clarity. As in the cubic case, the incoming resonances are stronger than the outgoing ones. This result is in agreement with the approximation reported in [2]. The remarkable intensity drop observed around 2.455 eV is due to interference effects between the outgoing resonances of the lh and hh excitons, higher order terms of incoming hh resonances and the continuum contribution. Less pronounced interference effects also occur around 2.42 eV between incoming lh and hh resonances. On the other hand, the low intensity observed for the lh exciton, as compared with the hh one, is mainly due to the smaller values of matrix elements involved in that resonance, as shown in table 1. Interference effects account for the difference between the intensity of the resonance in the cubic case and the sum of lh + hh resonances.

Interference effects have often been observed in the resonance profile of LO phonons in cubic semiconductors, and reproduced in the calculations of the Raman polarizability [2, 3, 16–18]. They are basically of two types: between allowed (DP) and forbidden (FI) scattering, and, for a given e–phonon interaction mechanism, between different excitonic resonances, such as those taking place at E_0 and $E_0 + \Delta_0$ critical points or between incoming and outgoing resonances. The interference between DP and FI scattering has the added interest that it allows one to quantify the relative contribution of intrinsic and extrinsic (impurity induced) processes to Fröhlich scattering [16]. In our case, the geometrical configurations chosen for the calculations do not allow for interference between DP and FI contributions, since either one or the other is inactive. As regards interference between excitonic resonances, the tetragonal splitting between lh and hh states gives rise to interference effects not observed in the cubic case. On the other hand, the large value of Δ_0 (403 meV) makes interference between (lh, hh) and so resonances negligible. We can get more insight into the origin of these effects in figure 2 by looking at the signs of the terms being summed in the calculation of the Raman polarizability for the DP interaction (equation (7)). Since the dominant term is the discrete–discrete one, to simplify the discussion we shall neglect the continuum contribution. Moreover, from the discrete–discrete term, we retain only the first excited states ($n = 1$) of lh and hh excitons, whose energies are $E_{lh,in} = 2.418$, $E_{hh,in} = 2.435$, $E_{lh,out} = 2.453$ and $E_{hh,out} = 2.47$. These energies define five regions: (1) $E < E_{lh,in}$, (2) $E_{lh,in} < E < E_{hh,in}$, (3) $E_{hh,in} < E < E_{lh,out}$, (4) $E_{lh,out} < E < E_{hh,out}$, (5) $E_{hh,out} < E$. Since K^{DP}_{qp} has the same sign for all q, p indices, the sign of each (p, q) term is just that of the denominator products $\eta'_p(\eta'_q - \eta_0)$, where the prime means that the corresponding gaps are diminished by the Rydberg energies and we have assumed, for the discussion, $\gamma_{p,q} \to 0$. It is straightforward to see that the signs of the two factors in each of these regions are (−−, +−, +−, +−, ++) and (−−, −−, +−, ++, ++) for ($p =$ lh, $q =$ hh) and ($p =$ hh, $q =$ lh) terms, respectively. By simple inspection we find that destructive interference will occur in the second and fourth regions, that is between lh and hh (incoming) and between lh and hh (outgoing) resonances, as reflected in the calculations.

Figure 3 illustrates the resonance of the dipole-allowed DP Raman scattering for modes B_{LO} and E_{LO} in the $\bar{z}(x, y)z$ and $\bar{x}(y, z)x$ backscattering configurations, respectively. The main difference appears in the region of outgoing resonance of lh and hh excitons where interference effects are produced, as previously discussed. In these calculations the broadening parameters have been given more realistic values, close to those typical of zinc-blende compounds: $\Gamma_{lh} = \Gamma_{hh} = 5$ meV; $\Gamma_{so} = 10$ meV. This makes the details of the profile much less resolved than in figure 2. In practice, the small CF splitting, for instance, may be undetectable.

Figure 4 shows the resonance of the dipole-forbidden FI Raman scattering for the B_2 mode in the $\bar{z}(x, x)z$ configuration in the tetragonal and cubic symmetries. Only the positions of $n = 1$ excitons have been indicated. As in figure 2, small Γ s are imposed so as to differentiate more clearly the contributions of each of the excitonic bands. Similarly to the DP interaction case, in the region of lh and hh excitons the peaks appear, in the cubic case, in the unsplit positions. The higher intensities of the hh peaks relative to lh ones are due to the difference between the effective masses m_{lh} and m_{hh} appearing in K_p^F ($m_{lh} \approx m_e$ while $m_{hh} \gg m_e$), the values of the matrix elements (see table 2) and interference effects. This results in the apparent gap shifting toward E_{hh}. Contrary to the DP case, in FI scattering the discrete–continuous terms are important and an analytical discussion of the origin of the interference effects is not as simple as in the DP case.

In figure 5 the resonances of the dipole-forbidden FI scattering for modes B_{LO} in $\bar{z}(x, x)z$ configurations and E_{LO} in $\bar{x}(z, z)x$ configurations are compared, using the same broadening parameters as in figure 3. E_{LO} in the $\bar{x}(y, y)x$ configuration gives results identical to those for B_{LO} in the $\bar{z}(x, x)z$ configuration. According to the matrix elements given in table 2, all excitons contribute to B_{LO} resonance in the $\bar{z}(x, x)z$ configuration, while only lh and so excitons are expected for E_{LO} in the $\bar{x}(z, z)x$ configuration. The low intensity of lh excitons, as in figure 4, is due to the small value of the factor $m_e - m_{lh}$ appearing in K_P^F (see table 3). Since the matrix element for hh excitons is zero for E_{LO} in the $\bar{x}(z, z)x$ configuration, the intensity in this configuration is much lower than for the B_{LO} mode. It is interesting to note that the mass effect is also expected in the cubic case, which means that, if electron and lh effective masses are very similar, the resonance in the lh + hh region will be almost entirely due to hh excitons.

In the so region all incoming and outgoing resonances are indicated. As compared with figure 4, the intensity maxima in this region are shifted toward the energies of $n = 2$ excitons. This is a consequence of the application of equation (12) for the broadening parameters $\Gamma_{so}(n)$. For $\Gamma_{so}(k) = 10$ meV and $\Gamma_{so}(1) = 10$ meV (figure 5) all excitons contribute with the same linewidth, while on taking $\Gamma_{so}(1) = 2$ meV (figure 4) the peak intensity of the $n = 1$ exciton is enhanced.

5. Summary and conclusions

The one-phonon RRS by high energy LO phonons of tetragonal zinc-blende-like semiconductors has been investigated, in the framework of a theoretical model including excitons as intermediate states and exciton–phonon interaction through deformation potential and Fröhlich mechanisms. With little modification the model can be applied to several families of tetrahedral semiconductors, such as II–III_2–VI_4 ordered-vacancy compounds and chalcopyrites. $ZnGa_2Se_4$ has been chosen as an example. Selection rules and interference effects for quasicubic B_{LO} and E_{LO} modes in different backscattering configurations have been analysed. The model depends and can give information on physical parameters such as the energy band gap, crystal field splitting, phonon mode energy and effective masses. The similarities and differences between our results and those for the cubic case are discussed.

Acknowledgment

J M Bergues acknowledges financial support from the Spanish Secretaría de Estado de Educación y Universidades.

References

[1] Cardona M 1982 *Light Scattering in Solids II* (*Springer Topics in Applied Physics* vol 50) ed M Cardona and G Güntherodt (Berlin: Springer)
[2] Cantarero A, Trallero-Giner C and Cardona M 1989 *Phys. Rev.* B **39** 8388
[3] Trallero-Giner C, Cantarero A and Cardona M 1989 *Phys. Rev.* B **40** 4030
[4] Cantarero A, Trallero-Giner C and Cardona M 1989 *Phys. Rev.* B **40** 12290
[5] Limmer W, Leiderer H, Jakob K, Gebhardt W, Kauschke W, Cantarero A and Trallero-Giner C 1990 *Phys. Rev.* B **42** 11325
[6] Limmer W, Bauer S, Leiderer H, Gebhardt W, Cantarero A, Trallero-Giner C and Cardona M 1992 *Phys. Rev.* B **45** 11709
[7] Choi I H and Yu P Y 1994 *Phys. Rev.* B **49** 16407
[8] Bacewicz R, Lottici P P and Razzetti C 1979 *J. Phys. C: Solid State Phys.* **12** 3603
Lottici P P and Razetti C 1983 *Solid State Commun.* **46** 681
Attolini G, Bini S, Lottici P P and Razetti C 1992 *Cryst. Res. Technol.* **27** 685
Razzetti C, Lottici P P and Bacewicz R 1982 *J. Phys. C: Solid State Phys.* **15** 5657
Ursaki V V, Burlakov I I, Tiginyanu I M, Raptis Y S, Anastassakis E and Anedda A 1999 *Phys. Rev.* B **59** 257
Sanjuán M L and Morón M C 2002 *Physica* B **316/317** 565
Allakhverdiev K, Gashimzade F, Kerimova T, Mitani T, Naitou T, Matsuishi K and Onari S 2003 *J. Phys. Chem. Solids* **64** 1597
[9] Neumann H 1991 *Cryst. Res. Technol.* **26** 1001
[10] Miller A, MacKinnon A and Weaire D 1981 *Solid State Phys.* **36** 119
[11] Shay J L and Wernick J H 1975 *Ternary Chalcopyrite Semiconductors: Growth Electronic Properties, and Applications* (London: Pergamon)
[12] Pollak F H and Cardona M 1968 *Phys. Rev.* **172** 816
[13] Ganguly A K and Birman J L 1967 *Phys. Rev.* **162** 806
[14] Elliot R J 1957 *Phys. Rev.* **108** 1384
[15] Yu P Y and Cardona M 1995 *Fundamentals of Semiconductors in Physics and Materials Properties* (Berlin: Springer) chapters 3 and 4
[16] Menéndez J and Cardona M 1985 *Phys. Rev.* B **31** 3696
[17] Kauschke W, Mestres N and Cardona M 1987 *Phys. Rev.* B **36** 7469
[18] Rösch M, Atzmüller R, Schaack G and Becker C R 1994 *Phys. Rev.* B **49** 13460
[19] Kerimova T G and Sultanova A G 2002 *Neorg. Mater.* **38** 1181